Sample exchange by beam scanning with applications to noncollinear pump–probe spectroscopy at kilohertz repetition rates

Austin P. Spencer, Robert J. Hill, William K. Peters, Dmitry Baranov, Byungmoon Cho, Adriana Huerta-Viga, Alexa R. Carollo, Anna C. Curtis, and David M. Jonas

Citation: Review of Scientific Instruments **88**, 064101 (2017); doi: 10.1063/1.4986628
View online: http://dx.doi.org/10.1063/1.4986628
View Table of Contents: http://aip.scitation.org/toc/rsi/88/6
Published by the American Institute of Physics

Sample exchange by beam scanning with applications to noncollinear pump–probe spectroscopy at kilohertz repetition rates

Austin P. Spencer,[1,a)] Robert J. Hill,[2,b)] William K. Peters,[1,c)] Dmitry Baranov,[1] Byungmoon Cho,[1,d)] Adriana Huerta-Viga,[1,e)] Alexa R. Carollo,[1] Anna C. Curtis,[1] and David M. Jonas[1,f)]

[1]*Department of Chemistry and Biochemistry, University of Colorado, Boulder, Colorado 80309-0215, USA*
[2]*Department of Physics, University of Colorado, Boulder, Colorado 80309-0390, USA*

(Received 9 March 2017; accepted 6 June 2017; published online 26 June 2017)

In laser spectroscopy, high photon flux can perturb the sample away from thermal equilibrium, altering its spectroscopic properties. Here, we describe an optical beam scanning apparatus that minimizes repetitive sample excitation while providing shot-to-shot sample exchange for samples such as cryostats, films, and air-tight cuvettes. In this apparatus, the beam crossing point is moved within the focal plane inside the sample by scanning both tilt angles of a flat mirror. A space-filling spiral scan pattern was designed that efficiently utilizes the sample area and mirror scanning bandwidth. Scanning beams along a spiral path is shown to increase the average number of laser shots that can be sampled before a spot on the sample cell is resampled by the laser to ~1700 (out of the maximum possible 2500 for the sample area and laser spot size) while ensuring minimal shot-to-shot spatial overlap. Both an all-refractive version and an all-reflective version of the apparatus are demonstrated. The beam scanning apparatus does not measurably alter the time delay (less than the 0.4 fs measurement uncertainty), the laser focal spot size (less than the 2 μm measurement uncertainty), or the beam overlap (less than the 3.3% measurement uncertainty), leading to pump–probe and autocorrelation signal transients that accurately characterize the equilibrium sample. [http://dx.doi.org/10.1063/1.4986628]

I. INTRODUCTION

In time-resolved optical spectroscopies, sequences of pulses, each sequence representing a complete and independent experiment, are repeated in order to record a transient which contains data as a function of the time delay(s) between pulses. Repetitive excitation artifacts come about when excited chromophores do not have adequate time to relax to thermal equilibrium with the bath before being probed again. In such a case, long-lived intermediates can influence or even dominate the dynamics observed in a variety of molecular systems.[1–4] For example, photon echoes can be stimulated from a frequency grating built up by repetitively exciting the sample.[5]

In order to increase the duty cycle of data collection without inducing such artifacts, techniques that exchange the sample within the probed volume are needed. Sample exchange, refreshing, or renewal techniques can be characterized by two key rates: a sample exchange rate and a resampling rate. The sample exchange rate is the rate at which the portion of sample excited by the previous laser shot is moved out of the laser focal spot. The resampling rate is the rate at which previously excited portions of the sample are revisited by the laser focal spot. To prevent repetitive excitation artifacts, the sample exchange rate should be greater than the laser repetition rate and the resampling rate should be less than the slowest sample relaxation rate. Techniques for sample exchange involve either moving the sample with respect to stationary laser beams (sample cell spinning,[1,6–10] translating,[4,11–13] flowing,[2–4,11,14–16] and stirring[17]), or moving the laser beams with respect to a stationary sample cell (spinning lens[18]). Moving-sample techniques often provide sufficient sample exchange but impose restrictions on the format of the sample cell. Conversely, a moving-beam technique, such as using a spinning lens to scan a circular pattern on the sample,[18] enables flexibility in choice of sample cell. Critically, moving the beams rather than the sample provides a means to rapidly refresh the sample between laser shots in cryostats and solid samples.

We present a sample exchange technique that extends the moving-beam strategy[18] by quickly scanning two crossing laser beams in a space-filling pattern such that each pulse sequence probes a portion of the sample not excited by prior pulses, taking advantage of the area of the sample cell to maximize resampling time. The advantages of this technique include average resampling rates on the order of 6 s^{-1} at 10 kHz laser repetition rate, low shot-to-shot spatial overlap, flexibility in sample cell format (rectangular, cylindrical, cryostat,

a)Current address: Department of Chemistry, Northwestern University, Evanston, Illinois 60208-3113, USA.
b)Current address: Intel Corporation, 2501 NW 229th Ave., RA3-353, Hillsboro, Oregon 97124, USA.
c)Current address: JILA, University of Colorado, Boulder, Colorado 80309, USA.
d)Current address: Korea University, Seongbuk-gu, Seoul 02841, South Korea.
e)Current address: Division of Chemistry and Biological Chemistry, Nanyang Technological University, Singapore 637371.
f)Author to whom correspondence should be addressed: david.jonas@colorado.edu

etc.), and interferometric stability. Compared to flowing or stirring, which requires only one scatter-free spot on the sample cell, sensitivity to light scattering points over the entire probed area is a disadvantage. Also, because the probe beam's direction heading onto the detector is not constant in the approach presented here, beam pointing compensation by an additional scanning mirror after the sample would be needed for probe beam detection using a spectrograph (see supplementary material). The scanning beam method developed here could be combined with moving-sample techniques to achieve even longer resampling times.

II. BEAM SCANNING DESIGN

A. Refractive optics implementation

The refractive-optics beam scanning apparatus in Fig. 1 is constructed using only commercially available equipment, of which the core is a fast steering mirror (FSM-300, Newport) and its controller/driver (FSM-CD300B, Newport). The FSM has a front-surface gimbaled, 1 in. diameter, enhanced aluminum-coated mirror whose angle is independently controlled about two orthogonal axes by four voice coils,[19–21] a type of linear actuator. It has a mechanical angular range of ±1.5°, a repeatability of ≤3 μrad, and a closed-loop amplitude bandwidth of ≥800 Hz. Since the FSM is designed for beam stabilization and scanning applications, for which speed and precision are critical, it is well suited to the needs of sample exchange. Compared to dual-axis galvanometer–based systems, which use two separate mirrors in a z-fold–like arrangement,[22] a voice coil–actuated FSM translates the reflected beams less while scanning, leading to a simpler optical setup and reducing aberrations in focusing all beams to the same spot within the sample.

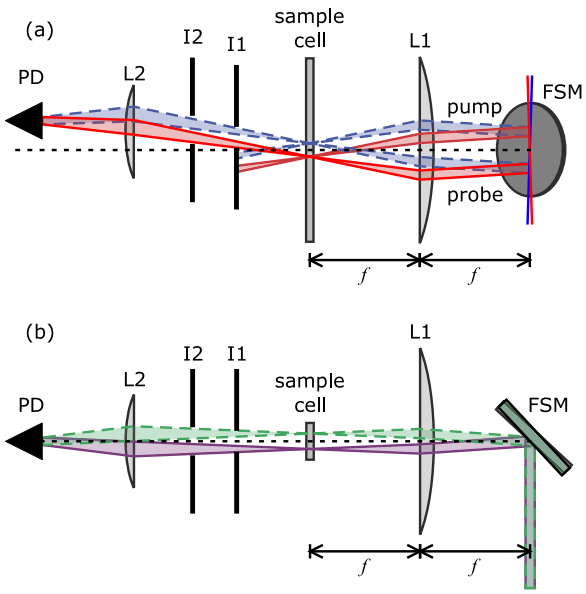

FIG. 1. Schematic of the refractive-optics beam scanning apparatus. Beams propagate from right to left, encountering a fast steering mirror (FSM), focusing lens (L1), sample cell, two irises (I1 and I2), collimating lens (L2), and photodiode (PD). The fast steering mirror (FSM) utilizes a 1 in. diameter aluminum-coated mirror. The focusing lens, L1, is a 2 in. diameter anti-reflection-coated (AR-coated) plano-convex lens with a 30 cm focal length, denoted by the distance f in the schematic. The sample cell is 5 cm × 1 cm with a 1 mm path length. The collimating lens, L2, is a 1 in. diameter AR-coated plano-convex lens with a 25 cm focal length. The photodiode, PD, is a biased silicon PIN photodiode detector which has a large active area diameter (4.57 mm). (a) Side view showing beams deviated up (dashed, blue) and deviated down (solid, red). (b) Top down view showing beams deviated left (solid, purple) and deviated right (dashed, green).

The optical layout is very similar to typical apparatus for laser scanning microscopy.[23] The FSM reflects two parallel beams, vertically offset by 1.2 cm, at 45° to the surface of the mirror. The vertically stacked beam geometry is necessary since it enables pump and probe beams to arrive at a common focus in the sample, largely independent of FSM deflection angle (see Sec. IV and the supplementary material).

An anti-reflection–coated (AR-coated) 2 in. diameter plano-convex lens (f = 30 cm) is centered in the path of the reflected beams at a distance of its focal length from the FSM. The distance between the FSM and lens is important because it controls the incident angle of the focused beams on the focal plane, in which the sample cell lies. In geometric optics, any ray emanating from the focal point of a lens will propagate parallel to the optical axis once it has passed through the lens.[24] Therefore, when a lens is placed such that its focal point coincides with the center of the FSM, the angle bisector between the focused beams will, neglecting the effects of optical aberrations,[25] fall normal to the focal plane in the sample for all deflection angles of the FSM. This, along with aligning the sample cell parallel to the focal plane, ensures constant optical path length through the sample cell as well as constant reflective losses from the sample cell interfaces.

Past the sample cell are two irises that are centered on the probe beam and are closed as far as possible without clipping the probe beam at any point in its scan pattern. The irises are used to block the pump beam and light scattered by the sample. They are positioned 20 cm and 32 cm from the sample cell, by which point the pump and probe scan patterns are spatially separated for a scan pattern whose diameter in the focal plane is 3 mm.

Beyond the second iris, there is an AR-coated 1 in. diameter plano-convex lens (f = 25 cm) that is placed 48 cm from the sample cell and centered on the probe beam, approximately 0.5 cm above the optical axis of the focusing lens. This lens serves to loosely focus the probe scan pattern onto a photodiode (ET-2040, Electro-Optics Technology; reverse-biased silicon PIN photodiode; 4.57 mm active area diameter) placed 25 cm beyond. Empirically, the photodiode surface is positioned on a plane in which the scanning beam is stationary; this plane is slightly before the focus, which is not stationary.

The location of the common focus for the two beams in the sample cell is controlled by the deflection angle of the FSM which is, in turn, controlled by two input voltages: one for the x (horizontal) deflection angle and one for the y (vertical) deflection angle. The FSM is capable of producing an arbitrary scan pattern on the sample cell, within its mechanical constraints on maximum deflection angle (±1.5°, mechanical) and bandwidth. Specifically, the FSM-300 can utilize its full angular range up to a frequency of 40 Hz, beyond which the maximum deflection angle is inversely proportional to the square of

frequency due to thermal loading of its drive coils.[26] For example, when the focal length of L1 is 20 cm and scanning a circular pattern with a 3 mm radius, the maximum scan velocity achievable by the FSM-300 is 1.38 m/s, enabling center-to-center separation of laser focal spots of up to 138 μm (1.38 mm) for a 10 kHz (1 kHz) laser repetition rate. The FSM-300's ±1.5° maximum mechanical deflection angle translates into a maximum pattern radius of 10.5 mm for the same 20 cm L1 focal length.

A trade-off exists between the maximum size of the scan pattern and the focal spot size of the laser at the sample. While a longer focal length for L1 allows for a larger scan pattern, it also increases the diffraction-limited focal spot size of the laser.[27] Since both the maximum scan pattern size and the focal spot size increase linearly with the focal length of L1, the maximum resampling time cannot be increased in this way. On the other hand, increasing the collimated beam waist *can* enable longer resampling times by decreasing the focal spot size. However, the collimated beam waist is necessarily restricted to $w_c < D/2 - \Delta/2$ (where Δ is the distance between collimated pump and probe beams) by the diameter of the FSM, D. The collimated beam waist is further restricted to $w_c < \Delta/2 - f\ \tan[\theta_{\max}]$ (where f is the focal length of L1 and $\theta_{\max}$ is the maximum FSM deflection angle in the scan pattern) by the significant margin needed to selectively block the pump with iris I2 and is also restricted by complicated factors influencing the nonlinear-signal to noise ratio. The maximum number of scan points before resampling is given by

$$N_{\max} = \frac{\pi^2 w_c^2 \tan^2(\theta_{\max})}{\lambda^2}, \tag{1}$$

where λ is the laser wavelength. For example, for a 2.5 mm collimated beam waist, a maximum deflection angle of ~0.29° (3 mm diameter scan pattern and 30 cm focal length), and 800 nm wavelength light, $N_{\max} = 2410$. This geometrical maximum does not consider frequency bandwidth constraints of the scanning mirror.

A refractive beam scanning apparatus with optics that are symmetric about the sample cell is proposed in the supplementary material. In this "ideal" implementation, use of equal focal length lenses on each side of the sample cell is expected to reduce the influence of scanning artifacts (e.g., non-stationary probe beam on the detector).

B. Reflective optics implementation

An all-reflective-optics version of this beam scanning apparatus was also constructed (Fig. 2) and has the advantage of eliminating the dispersion and chromatic aberration caused by refractive optics at the cost of added astigmatism. The primary difference is in the use of 2 in. diameter spherical concave mirrors (f = 20 cm, Thorlabs CM508-200-P01) instead of lenses. In order to minimize optical aberrations, the FSM and curved mirrors are used at near-normal incidence. In terms of layout and alignment, the same guiding principles that were used with the refractive optics setup were used here. Just as in the refractive implementation, the sample cell is placed perpendicular to the optical axis of the focusing mirror so as to coincide with its focal plane. However, with the near-normal incidence layout, this must be accomplished in a different way (see supplementary material). Likewise, the optical axis of the collimating mirror after the sample lies parallel to that of the focusing mirror. As in the refractive implementation, the first iris after the sample is placed far enough away that it is able to fully block the pump beam while transmitting the probe beam over the entire scan pattern.

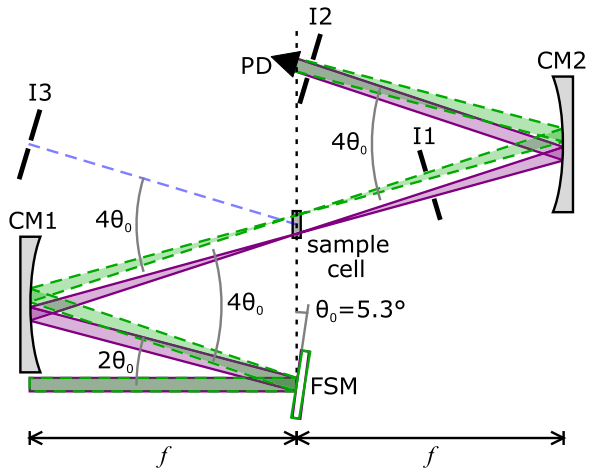

FIG. 2. Top-down view of the all-reflective-optics beam scanning apparatus (*not* drawn to scale—the angle θ_0 is greatly exaggerated). Beam paths for two different FSM deflection angles are illustrated: left (solid, purple) and right (dashed, green). Only one beam is visible for each FSM deflection angle when viewed from above since the pump and probe beams are vertically offset. Beams start at the bottom-left of the diagram, travelling from left to right, encountering (in order) a fast steering mirror (FSM), spherical concave mirror (CM1), sample cell, iris (I1), spherical concave mirror (CM2), iris (I2), and photodiode (PD). Both concave mirrors are aligned such that they share a common focal plane, in which lies the FSM, the sample cell, and the front face of the detector. The concave mirrors (CM1 and CM2) have a 2 in. diameter, 20 cm focal length (denoted by the distance f in the schematic), and are protected-silver coated. The sample cell is 5 cm × 1 cm with a 1 mm path length. The photodiode, PD, is a biased silicon PIN photodiode detector with a large active area diameter (4.57 mm).

III. SCAN PATTERN

The three primary goals in formulating a scan pattern were to (1) decrease as much as possible the rate at which spots in the sample cell are revisited by the laser, (2) minimize shot-to-shot spatial overlap of successive sequences of laser pulses, and (3) avoid driving the FSM beyond its mechanical limitations. These requirements eliminate certain approaches, including rastering line-by-line, which cannot simultaneously satisfy goals 2 and 3 above for the experimental conditions of interest because the large bandwidth needed to reverse the mirror's angular motion when moving from one scan line to the next would cause the FSM to exceed the current limit of its voice coils. An effective solution to these goals is a bidirectional space-filling spiral pattern. As depicted in Fig. 3, this pattern closely resembles an Archimedean spiral with laser shots spaced at a constant distance d along the path of the spiral, starting at some minimum radius and moving outward. Once the defined maximum radius is reached, the radial velocity is reversed (but not the tangential velocity) such that the beams are spiraled back to the minimum radius. This pattern assures

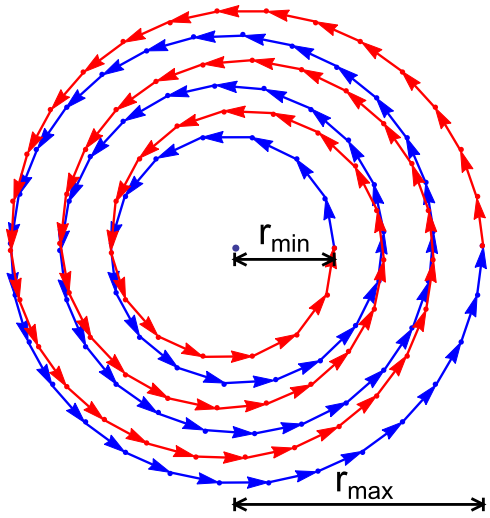

FIG. 3. A space-filling spiral pattern consists of an outward-traveling spiral (blue) followed by an inward-traveling spiral (red). Dots indicate the location of laser shots on the sample while arrows show the direction of travel between laser shots. The pattern obeys boundary conditions specifying the minimum (r_{min}) and maximum (r_{max}) radii. Each laser shot is separated (tangentially) by a distance d from the prior (and subsequent) laser shot. Likewise, after each 360° cycle within the pattern, laser shots are displaced radially by the distance d. For clarity, this schematic exaggerates d so that there are only 3 cycles between r_{min} and r_{max}. Experiments had ~20 cycles in each of the inward- or outward-traveling spirals.

that the centers of successive laser shots are separated by a controlled distance, d. Considering only an outward- or inward-traveling section of the pattern, laser shots from one angular period of the scan pattern to the next are also separated by the same distance d. The space-filling spiral pattern has the advantage of constant shot-to-shot spatial overlap and effective use of sample cell area, which is important for achieving low resampling rates. The minimum radius parameter allows for better control of resampling rate and for avoidance of the center part of the pattern where the angular frequency necessary to maintain the center-to-center spacing d can surpass the bandwidth limitations of the FSM. The disadvantage of the bidirectional spiral scan pattern is that the outward- and inward-traveling spirals overlap to some extent at various points within each pattern.

This pattern was implemented by setting a constant tangential speed $v_{tan} = dk_{laser}$, where k_{laser} is the laser repetition rate and setting the radial speed to $v_{rad}(t) = df_{tan}(t)$, where $f_{tan}(t) = v_{tan}/2\pi r(t)$ is the tangential cyclic frequency, v_{tan} is the tangential speed, and $r(t)$ is the radius of the pattern at time t (see supplementary material for details). The number of spots contained within half (either the outward or inward traveling portion) of the space-filling spiral pattern matches that predicted by square packing of circular focal spots within the area of the scan pattern (i.e., the number of spots in the pattern is given by the area of the scan pattern divided by the squared spot separation); a more complicated scan with hexagonal packing might allow up to ~15% improvement. While the scanned path is cyclical (i.e., repeats exactly), the location of laser shots on the continuously scanned curve need not coincide exactly between cycles of the scan pattern. The locations of laser shots will perfectly repeat only if the period of the scan pattern is an exact integer multiple of the laser repetition period (see supplementary material).

Motion of the FSM is computer controlled, enabling rapid customization of the scan pattern based on experimental requirements. A LabVIEW program calculates the scan path and outputs its x and y coordinates as voltages through a sound card. These voltages serve as the control signals for the two rotation axes of the FSM.

IV. CHARACTERIZATION

After the scan pattern was verified using photosensitive paper, characterization of the refractive setup required measurements of how laser spot size, pump–probe overlap, pulse duration, and pump–probe delay vary during beam scanning. Scanning the FSM did not cause vibrations that would prevent use of an interferometer while scanning (see supplementary material). The laser focal spot was imaged in the focal plane as a function of FSM deflection angle using an imaging sensor (ZoomCam USB Model 1598 with lens removed; see supplementary material). Placement of the imaging sensor in the focal plane is described in the supplementary material. The resulting images of pump and probe beams were fit with a 2D elliptical Gaussian to extract the spot widths [44 μm full-width at half-maximum (FWHM)], which varied by less than 4% for either beam over the full ~2 mm square sampled scanning area. Since the measured spot width varies by as much as 6% depending on how well the imaging sensor is placed in the focal plane, 4% should be viewed as an upper bound on the position-dependent spot width variation. The 2D Gaussian fits also indicate the positions of pump and probe focal spots at each FSM deflection angle, enabling changes in relative spot position to be quantified. Relative spot position is defined as the spatial separation between pump and probe beam centers in the plane of the imaging sensor. For the same range of FSM deflection angles as above, the root-mean-square (RMS) deviation of the relative spot position (as a percentage of the full-width at half-maximum of the focal spot) was 8.2% in the horizontal dimension and 14.5% in the vertical dimension, both of which are within the precision of this measurement (~15.5%), which is limited by the estimated ±2.5° accuracy of placing the imaging sensor in the focal plane. Assuming that a change in relative beam position is the result of a change in the z-position of the pump–probe crossing point relative to the surface of the imaging sensor, a 14.5% change in the relative spot position corresponds to a 163 μm change in the relative z-position for the refractive implementation depicted in Fig. 1. This is a relatively small distance compared to not only the sample path length (1 mm) but also the crossing length of the beams (2.25 mm) and the Rayleigh range (5.74 mm). In addition, changes in relative beam position in the plane of the imaging sensor can result from optical aberrations in the focusing optics, which cause the z-position of the focus to vary with FSM deflection angle.

Given the measured change in relative spot position, the change in beam overlap is calculated from the spatial profiles for the pump and probe beams at the focus (see supplementary material). For beams with a circular Gaussian spatial profile

and a FWHM spot size of 44 μm, a 15.5% change in the relative spot position corresponds to a 3.3% decrease in overlap between pump and probe beams compared to perfectly overlapped beams. Since the pump–probe signal is proportional to this overlap, variations induced by scanning are attenuated by an electronic frequency filter prior to further processing (e.g., lock-in amplification).

To ensure that beam scanning does not alter transient measurements beyond reducing repetitive excitation, autocorrelations and pump–probe transients were acquired under both scanning and stationary beam conditions for comparison. These measurements are sensitive to changes in pump–probe pulse delay, spatial overlap and the incident angle at the sample, and probe pulse detection efficiency. Changes in any of these properties caused by beam scanning would distort the resulting transients and introduce artifacts.

An intensity-detected second-order noncollinear autocorrelation (Fig. 4) was measured in the refractive beam scanning apparatus both with the FSM held at a constant deflection angle and with the FSM performing the space-filling spiral pattern. Autocorrelations were recorded from −400 fs to 400 fs with 5 fs time steps. Two scans were acquired under both scanning- and stationary-beam conditions, enabling the measurement uncertainty to be estimated and compared to the variations caused by beam scanning. The maximum possible pattern size with the 5 mm diameter beta-barium borate (BBO) crystal was used, and the resulting autocorrelation showed no apparent difference compared to the stationary-beam autocorrelation. The RMS deviation (see supplementary material) between scanning- and stationary-beam autocorrelations was 0.34%, which is less than the 0.39% deviation between two stationary-beam autocorrelations taken under equivalent conditions. Fitting a Gaussian function to the autocorrelations from $T = -100$ fs to 100 fs gives differences between the scanning- and stationary-beam autocorrelations of 1.2% in maximum signal, 0.074 fs in time zero, and <0.1 fs in autocorrelation width. The same comparison applied to two equivalent stationary-beam autocorrelations yields a difference of 0.4% in maximum signal, 0.42 fs in time zero, and 0.27 fs in autocorrelation width.

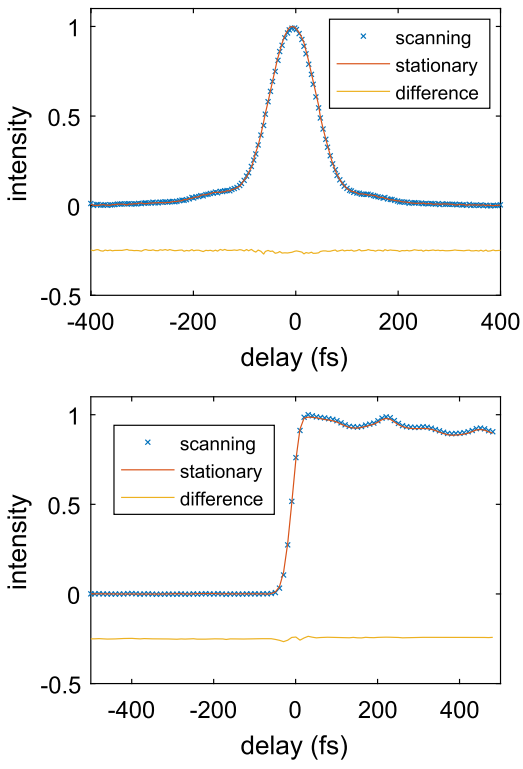

FIG. 4. Comparisons between scanning and stationary beam transients. Second-order autocorrelations recorded using the refractive beam scanning apparatus with 75 fs duration pulses (top panel) agree within their uncertainty. Pump–probe transients of IR-125 recorded using the reflective beam scanning apparatus with 28 fs pulses (bottom panel) are 0.7% ± 0.4% (uncertainty is the standard deviation) larger under scanning than stationary beam conditions, as expected based on the repetition rate, excitation probability, photoproduct yield, and photoproduct lifetime. The difference between scanning and stationary beam transients is offset by −0.25 for clarity.

To demonstrate that beam scanning does not distort their shape or amplitude, pump–probe transients (Fig. 4) of the laser dye IR-125 in ethanol were taken using the reflective beam scanning apparatus both with the space-filling pattern and with stationary beams. For the experimental conditions used here, which were chosen to minimize photoproduct buildup for stationary beams, the stationary beam measurement is expected to yield 0.8% less pump–probe signal than an equivalent measurement in the zero resampling rate limit due to the small buildup of a long-lived photoproduct when repetitively exciting the same sample volume (see supplementary material). The time step size was 10 fs and comparisons were restricted to pump–probe time delays between −500 fs and 500 fs. As with the autocorrelation measurements above, multiple (10 each) scans were acquired while alternating between scanning- and stationary-beam conditions to enable estimation of the measurement uncertainty. Since similar errors occur within each set, a 1.2 fs time zero shift was attributed to translation stage repeatability and removed. The resulting stationary-beam transient has 0.7% ± 0.4% (uncertainty is the standard deviation) lower signal, which agrees with the expected difference within the uncertainty. Importantly, the periodic scan pattern has not contaminated the pump–probe transient, as demonstrated by the precise replication of the multiple vibration quantum beat pattern between data sets.

It can be seen in Fig. 3 that the outward-travelling and inward-travelling spirals cross over one another several times within the pattern. This motivated further characterization of the bidirectional space-filling spiral pattern to quantify the effect of this intra-pattern focal spot overlap. First, the spatial and temporal coordinates of each focal spot within a single cycle of the pattern are calculated for a given set of pattern parameters. Second, the partial overlap $H_{i,j}$ between focal spots i and j in the scan pattern is calculated for integers i,j from 0 to $N - 1$. If the photoproduct buildup is small and can be approximated as linear in the pulse energy, one can average the partial overlaps with the same resampling time interval over all the different spots in the pattern. For a pattern with N focal spots, there are N resampling time intervals, each with an integer index, $n = j - i$, ranging from 1 to N in order of increasing duration. The partial overlaps for focal spot pairs with equal resampling time intervals are then averaged, yielding the average partial overlap at each resampling time interval

within the pattern,

$$H_n = \frac{1}{N}\sum_{i=0}^{N-1} H_{i,i+n}, \tag{2}$$

where $i + n$ is interpreted as $(i + n)$ modulo N.

The result of this analysis for typical experimental conditions is illustrated in Fig. 5. A pattern diameter of 3 mm mimics that of the experiment, wherein the pattern size was restricted in order to avoid light scattering defects on the sample cell, decreasing the number of spots in the spiral. The data point at the end of the pattern with a height of 1 is the "perfect" overlap that occurs between any two laser focal spots separated by one complete cycle of the pattern, and its value serves as a reference level for comparison to the average partial overlaps that occur at shorter intervals within a single cycle of the pattern. The second highest average partial overlaps, compared to the maximum at $n = N$, occur at $n = 1$ and $n = N - 1$. These points represent the shot-to-shot overlap between immediately subsequent focal spots and have equal values (~0.15) due to the cyclic average. This mirror symmetry extends to all points in the pattern and obeys the relationship $H_n = H_{N-n}$. Outside of the points at $n = 1$ and $N - 1$, no other resampling time interval has an overlap of more than 1.8% of the peak, and only 416 out of 5027 resampling time intervals have an average partial overlap of more than 0.1%. These low average partial overlaps mean that any high partial overlaps between individual pairs of spots (as can be seen in Fig. 3) are balanced out by many lower partial overlaps between other individual pairs of spots with the same resampling time interval. The sum of the partial overlaps in one complete cycle of this pattern is $\sum_{n=1}^{N} H_n = 3.17$. If a photoproduct has a lifetime much longer than the periodicity of the pattern, then the average resampling rate

$$k_{\text{resampling}} = k_{\text{pattern}} \sum_{n=1}^{N} H_n, \tag{3}$$

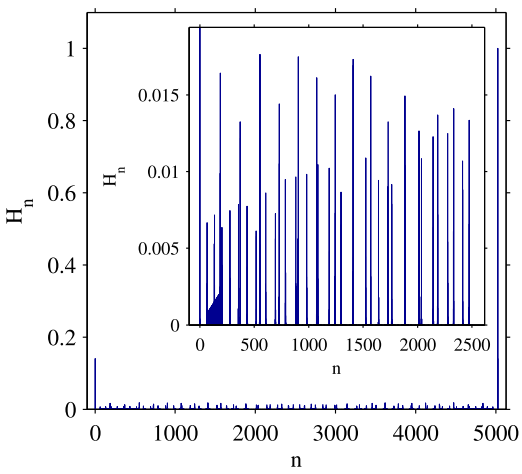

FIG. 5. A simulation of the average overlap H_n between laser focal spots at every resampling time interval index n during one cycle of the bidirectional space-filling spiral pattern ($n = 1, \ldots, N$). This particular pattern has 5027 points, a period of 0.503 s, and an average resampling rate of 6.30 s^{-1}. Center-to-center spot separation, $d = 50$ μm; laser repetition rate, k_{laser} = 10 kHz; full-width at half-maximum of Gaussian focal spot, $w_0^{\text{FWHM}} = 42$ μm; maximum spiral radius, $r_{\text{max}} = 1.5$ mm; desired minimum spiral radius, $r'_{\text{min}} = 0.5$ mm. The inset is a close-up view that shows the first half of resampling time intervals (up to $n = 2513$) since the two halves are mirror images.

where k_{pattern} is the pattern repetition rate, can be used to calculate a time-averaged photoproduct concentration. The average resampling rate approaches the pattern rate as the ratio of focal beam waist to spot separation goes to zero ($w_0^{\text{FWHM}}/d \to 0$). For the pattern in Fig. 5, the average resampling rate is 6.30 s^{-1}, which is about a factor of 3 faster than the pattern repetition rate $[(2t_{\text{max}})^{-1}]$ of 1.99 s^{-1}. On average, at 10 kHz this resampling rate corresponds to the accumulation of one perfect overlap after every 1700 shots. By comparison, a circular pattern (like that scanned by a spinning lens[18]) with the same radius and spot separation would yield a pattern repetition rate of 53.2 s^{-1} and an average resampling rate of 68.2 s^{-1}.

The choice of pattern parameters and laser spot size naturally depends on the system under study. If the sole concern is a long-lived excited state, then immediately subsequent pulse overlap can be minimized by decreasing w_0/d. On the other hand, one can minimize buildup of a minor photoproduct with a lifetime longer than the pattern period (e.g., quantum dots) by decreasing $k_{\text{resampling}}$. The above scan pattern was optimized for this purpose. The relatively high shot-to-shot partial overlap above is neutralized by phased lock-in detection at $k_{\text{laser}}/4$, which precisely cancels signals from the prior pump pulse and current probe pulse (for each cycle of 4 probe pulses, such signals occur once with the pump on and once with the pump off, and thus cancel).

In principle, scanning noncollinear beams over an area of the sample can cause variations in their relative time delay. While scanning the FSM in the horizontal symmetry plane (perpendicular to the plane containing the pump and probe beams) cannot cause a change in relative beam timing, vertical scanning (in the plane containing the pump and probe beams) can cause small changes in delay. A two-dimensional ray tracing simulation of pump and probe beam paths in the reflective optics implementation (for $r_{\text{max}} = 3$ mm, 2.9° beam crossing angle, and f = 20 cm) predicts only small variations in pump–probe delay (<0.16 fs) and focal surface flatness (<6 μm) over the full range of the scan pattern. This estimate should be accurate as long as the sample cell is aligned so that it contains the plane of maximum pump–probe overlap (for example, by the method described in the supplementary material) to within $\pm\sin^{-1}[L/(2r_{\text{max}})]$ (= ±9.6° for path length L = 1 mm and $r_{\text{max}} = 3$ mm). A variation in delay of 0.16 fs is less than 6% of a period of 800 nm wavelength light (2.67 fs), suggesting that sample exchange by beam scanning might be appropriate even for noncollinear spectroscopic techniques requiring interferometric stability of pulse delays, such as 2DFT spectroscopy.[28] In addition, 0.16 fs is much less than the calculated crossing-angle delay smearing[29] $\delta t = \alpha_0 w_0^{\text{FWHM}}/c = 3.5$ fs, where $2\alpha_0 = 2.86°$ is the crossing angle between beams, $w_0^{\text{FWHM}} = 42$ μm is the diameter of the beam focal spot, and c is the speed of light.

V. CONCLUSIONS

A new sample exchange technique that uses a computer-controlled fast steering mirror to scan laser beams across a sample cell was designed, constructed, and characterized for refractive and reflective optics. A bidirectional space-filling

spiral scan pattern enables low resampling rates (6.30 s^{-1} at k_{laser} = 10 kHz) with negligible partial overlaps while avoiding subsequent shot-to-shot overlap. Compared to the spinning lens technique,[18] which can probe a stationary sample around a circular path, the scanning beam approach can probe an annulus, thus allowing longer resampling times in stationary samples. Beam scanning has a negligible effect on pump–probe focal spots and timing. Ray tracing predicts less than 0.16 fs timing variation and measurements of these effects are all below measurement uncertainty (0.4 fs for timing variation). Time domain filtering, frequency domain filtering, and varying the data sampling rate were found to be valuable in mitigating noise from spatial variations of the sample. Shot-to-shot sample exchange at a laser repetition rate of 10 kHz was demonstrated and rates of up to 100 kHz are possible.

Sample exchange by beam scanning can limit repetitive excitation for sample cells of practically all sizes and shapes, enabling measurements for which it is either inconvenient or impossible to move the sample relative to the light source, such as cryostats and other bulky or heavy sample cells. The flexibility in scan pattern opens up the possibility of using the resampling rate as an adjustable experimental parameter to measure dynamics. In addition, beam scanning can be used in concert with other sample exchange techniques, such as flowing,[2–4,11,14–16] stirring,[17] translating,[4,11–13] or spinning,[1,6–10] to further slow the resampling rate without sacrificing shot-to-shot sample exchange.

SUPPLEMENTARY MATERIAL

See supplementary material for more information about: refractive setup optimization; the proposed ideal refractive implementation; reflective setup optimization; the scan pattern; sources of noise and noise mitigation; characterization of phase stability, pump–probe beam overlap, transient signals, and intra-pattern overlap; treatment of IR-125 relaxation; and extensions for use with multi-channel detection.

ACKNOWLEDGMENTS

The authors would like to thank Jisu Ryu for valuable contributions to the manuscript. This material is based upon work supported by the National Science Foundation under Grant No. CHE-1405050. Any opinions, findings, and conclusions or recommendations expressed in this material are those of the authors and do not necessarily reflect the views of the National Science Foundation. A.H.V. acknowledges support from CONACYT through a postdoctoral fellowship. A.R.C. is supported by the National Science Foundation Graduate Research Fellowship Program under Grant No. DGE-1144083.

[1] W. Kiefer and H. J. Bernstein, Appl. Spectrosc. **25**, 500 (1971).
[2] B. N. Toleutaev, T. Tahara, and H. Hamaguchi, Appl. Phys. B: Lasers Opt. **59**, 369 (1994).
[3] Y. Su and G. N. R. Tripathi, J. Am. Chem. Soc. **116**, 4405 (1994).
[4] J. Oberlé, E. Abraham, A. Ivanov, G. Jonusauskas, and C. Rullière, J. Phys. Chem. **100**, 10179 (1996).
[5] W. H. Hesselink and D. A. Wiersma, J. Chem. Phys. **75**, 4192 (1981).
[6] W. Xiao, S. Lin, A. K. W. Taguchi, and N. W. Woodbury, Biochemistry **33**, 8313 (1994).
[7] D. C. Arnett, C. C. Moser, P. L. Dutton, and N. F. Scherer, J. Phys. Chem. B **103**, 2014 (1999).
[8] B. M. Cho, C. F. Carlsson, and R. Jimenez, J. Chem. Phys. **124**, 144905 (2006).
[9] R. Fanciulli, I. Cerjak, and J. L. Herek, Rev. Sci. Instrum. **78**, 053102 (2007).
[10] D. Baranov, R. J. Hill, J. Ryu, S. D. Park, A. Huerta-Viga, A. R. Carollo, and D. M. Jonas, Rev. Sci. Instrum. **88**, 014101 (2017).
[11] T.-Q. Ye, C. J. Arnold, D. I. Pattison, C. L. Anderton, D. Dukic, R. N. Perutz, R. E. Hester, and J. N. Moore, Appl. Spectrosc. **50**, 597 (1996).
[12] E. G. Andrizhiyevskaya, D. Frolov, R. van Grondelle, and J. P. Dekker, Biochim. Biophys. Acta, Bioenerg. **1656**, 104 (2004).
[13] M. L. Groot, L. J. G. W. van Wilderen, and M. Di Donato, Photoch. Photobiol. Sci. **6**, 501 (2007).
[14] A. G. Midgett, H. W. Hillhouse, B. K. Hughes, A. J. Nozik, and M. C. Beard, J. Phys. Chem. C **114**, 17486 (2010).
[15] J. Bredenbeck and P. Hamm, Rev. Sci. Instrum. **74**, 3188 (2003).
[16] M. J. Tauber, R. A. Mathies, X. Chen, and S. E. Bradforth, Rev. Sci. Instrum. **74**, 4958 (2003).
[17] G. Nair, L.-Y. Chang, S. M. Geyer, and M. G. Bawendi, Nano Lett. **11**, 2145 (2011).
[18] D. Ionascu, F. Rosca, F. Gruia, A. Yu, and P. M. Champion, Rev. Sci. Instrum. **77**, 064303 (2006).
[19] O. Lodge, J. Inst. Electr. Eng. **27**, 799 (1898).
[20] A. G. Bell, "Improvement in telegraphy," U.S. patent 174465 (March 7, 1876).
[21] O. Gomis-Bellmunt and L. F. Campanile, *Design Rules for Actuators in Active Mechanical Systems* (Springer London, London, Dordrecht, Heidelberg, New York, 2010), pp. 3–28.
[22] M. M. Gabriel, J. R. Kirschbrown, J. D. Christesen, C. W. Pinion, D. F. Zigler, E. M. Grumstrup, B. P. Mehl, E. E. M. Cating, J. F. Cahoon, and J. M. Papanikolas, Nano Lett. **13**, 1336 (2013).
[23] P. Saggau, Curr. Opin. Neurobiol. **16**, 543 (2006).
[24] E. Hecht, *Optics*, 2nd ed. (Addison-Wesley, 1987).
[25] F. Jenkins and H. White, *Fundamentals of Optics*, 4th ed. (McGraw-Hill Science/Engineering/Math, 2001).
[26] Newport Corporation, "FSM-300 or FSM-320 fast steering mirror & FSM-CD300b controller/driver," User's Manual (Newport Corporation, 2003).
[27] A. E. Siegman, *Lasers*, 1st ed. (University Science Books, 1986).
[28] D. M. Jonas, Annu. Rev. Phys. Chem. **54**, 425 (2003).
[29] A. Baltuska, M. Pshenichnikov, and D. Wiersma, IEEE J. Quantum Electron. **35**, 459 (1999).